Configurational Dynamics of High Molecular Weight Polystyrenes in Good Solvents

Mamta Bhatt and Alex M. Jamieson*

Department of Macromolecular Science, Case Western Reserve University, Cleveland, Ohio 44106. *Received August 25, 1988; Revised Manuscript Received December 6, 1988*

ABSTRACT: Dynamic light scattering (DLS) measurements, over a wide range of qR_g, are reported for polystyrene (PS) samples of weight-average molecular weight $M_w = 8.42 \times 10^6$ and 20×10^6 in tetrahydrofuran (THF) and in ethylbenzene (ETBZ) at 25 °C. The DLS relaxation spectrum is successfully resolved into a slow mode corresponding to pure translational diffusion and a fast mode containing information on intramolecular motion, using a combination of multiexponential sampling and a restricted double-exponential fitting. The z-average translational diffusion coefficient, $D^0_{t,z}$, the longest intramolecular relaxation time, τ_1, and the fraction of the total scattering amplitude that resides in the translational diffusive mode, P_o/P, are determined as a function of the reduced scattering vector, $X^{1/2} = q\langle R_g\rangle^{1/2}$. The values characteristic of a single coil are obtained by extrapolation to infinite dilution. The τ_1 values for PS in ETBZ, corrected for solvent viscosity, are approximately 50% larger than those obtained in THF. In addition, at $X \gg 1.0$, the single-chain dynamic form factor, $P_o(X)/P(X)$, indicates that the contribution of the internal modes is considerably enhanced for PS in THF versus PS in ETBZ. These observations for τ_1 and $P_o(X)/P(X)$ suggest inherent differences in the nature of the internal chain hydrodynamics in these two good solvent systems, qualitatively consistent with the presence of a larger solvent draining effect for PS in ETBZ. Comparing our results with literature data, we suggest that the $P_o(X)/P(X)$ data plotted against the scaled quantity, $q^2R_h^2$, may be a universal function for different polymer solvent systems, independent of solvent quality.

Introduction

In recent years, the ability of modern dynamic light scattering instrumentation to resolve details[1] of the spectral distribution of scattered light has improved. Consequently, new interest has developed in the use of dynamic light scattering to investigate the intramolecular relaxations of flexible chains in good[2] and Θ[3,4] solvents. These and earlier[5-9] studies interpret the experimental results in the scattering wavevector regime, $qR_g > 1.0$, using a theoretical framework derived from the original analysis by Pecora[10-14] for a free-draining Gaussian chain. The spectrum of scattered light is shown to contain contributions from pure translational diffusion as well as intramolecular relaxations. The ratio of the amplitude of the diffusive mode to the total scattering amplitude, P_o/P, is predicted to depend uniquely on the parameter $X = q^2\langle R_g^2\rangle$, where q is the scattering wavevector and $\langle R_g^2\rangle$ is the z-average radius of gyration. For $X \ll 1.0$, only the pure translational mode contributes to the total scattered intensity, while for $X \gg 1.0$ the spectrum is composed of contributions from several modes arising from the flexing motions of the polymer chain. However, in an intermediate range of X, almost all of the scattered intensity is distributed between two modes of relaxation. The first mode is due to translational motion of the entire macromolecule and is an exponential decay whose frequency constant $\Gamma_1 = Dq^2$, where D is the translational diffusion coefficient. The second mode is an exponential decay that depends on the relaxation time, τ_1, of the first normal mode of motion and has a frequency constant $\Gamma_2 = (Dq^2 + 2/\tau_1)$. The relative amplitudes of these modes in the spectrum of scattered light have been predicted on the basis of dynamical models for the case of zero hydrodynamic interaction,[10-14] as well as various degrees of hydrodynamic interactions.[15,16] Theoretical predictions have also been made for the relaxation time, τ_1, associated with the first mode for the free-draining[17] limit and for intermediate levels of draining up to the nondraining limit.[18]

Following these theoretical considerations, previous experimental studies[2-9] have interpreted the spectrum of scattered light in the intermediate X region to obtain a value of τ_1 characteristic for a given polymer solvent system. Various methods of analysis can be applied to obtain τ_1, e.g., double-exponential[6-9] fits, histogram analysis,[2-5,19-21] and Laplace transformation using the method of constrained regularization[22-25] and multiexponential sampling analysis.[24-29] However, only a few[2-5] recent studies have been sufficiently detailed to test theoretical predictions.[10-14,16-18] In these experiments, appropriate extrapolations to infinite dilution and zero scattering angle were made to determine the value of the longest intramolecular relaxation time, τ_1, for a single chain. For polystyrene (PS) chains, conflicting results for τ_1 have been reported. Earlier experiments done on the marginal solvent system, PS in methyl ethyl ketone, and the Θ solvent cyclohexane[6,7a] yielded τ_1 values in agreement with values estimated from the free-draining Rouse model. Later studies[7b,8,9] on the same systems yielded τ_1 values in agreement with the nondraining Zimm prediction. However, none of these initial studies were performed over a wide range of concentrations and scattering angles, which facilitates appropriate comparison of theory and experiment.

Recently, such experiments have been performed in the good solvent system, PS[2] in benzene (BZ) and the Θ solvent system PS in *trans*-decalin (TD).[4,5] The τ_1 values deduced were reported, in each case, to be in good agreement with the Zimm model. Interestingly, however, experimental data for the single-chain dynamic form factor $P_o(X)/P(X)$ show substantial differences in these two solvent systems. A theoretical analysis predicts that $P_o(X)/P(X)$ should vary with the strength of the hydrodynamic interaction.[16] However, the effect of excluded volume on the light scattering data has not been evaluated.

It is pertinent to note here that the ratio of the static to dynamic radii, ρ $(=\langle R_{g,z}\rangle/\langle R_h^{-1}\rangle^{-1})$, for these solvent systems is different. For the good solvent, PS in BZ, the value obtained is $\rho \simeq 1.57$, comparable to experimental data in other good solvents.[30-32] For the Θ solvent, PS in TD, the value reported is $\rho \simeq 1.27$ in good agreement with ρ values determined in other Θ systems.[32] Several theoretical analyses of the hydrodynamics of flexible coils[33-36] interpret these different ρ values as indicating that there are different levels of solvent draining between Θ and good solvent systems, with the good solvent having a large draining effect. However, this point of view is controversial, and other theoretical treatments[32] conclude that these differences in ρ values between good and Θ systems

0024-9297/89/2222-2724$01.50/0

can be explained solely on the basis of excluded volume effects.

Static and dynamic light scattering experiments[37-39] in our laboratory have discovered that tetrahydrofuran (THF) and ethylbenzene (ETBZ) are solvents of comparable solvating power for PS and yet have significantly different ratios of the static to dynamic radii, ρ (= $\langle R_{g,z}\rangle/\langle R_h^{-1}\rangle^{-1}$). In particular, while PS/ETBZ has a value of $\rho \simeq 1.55 \pm 0.05$, similar to that observed for PS/BZ, PS/THF has $\rho \simeq 1.27 \pm 0.04$, comparable to those values obtained in Θ solvents. Actually, the experimental values of the interpenetration parameter, ψ,

$$\psi = A_2M^2/4\pi^{3/2}N_A\langle R_g^2\rangle^{3/2} \quad (1)$$

are significantly different in the two solvent systems. We determined $\psi = 0.21 \pm 0.02$ for PS in ETBZ and 0.32 ± 0.04 for the PS/THF system. Since theory predicts ψ to increase monotonically from zero at the Θ temperature to a positive asymptotic limit, we deduce that, if anything, PS/THF is closer to the good solvent asymptote than PS/ETBZ. Application of the porous sphere hydrodynamic theory[33,34] to the different ρ values led us to conclude that, in THF, polystyrene is less permeable to solvent than in ETBZ.[37-39] It is clearly of interest to perform dynamic light scattering studies at large scattering angles in these two good solvent systems to investigate whether differences in the intramolecular modes of motion due to variations in the nature of the internal chain hydrodynamics can be observed.

Thus, in this paper, we extend our dynamic light scattering analyses to large scattering vectors ($qR_g \gg 1.0$) where the effective decay rate, Γ_e, of the photon correlation function is influenced by internal (configurational) motions of the polystyrene chains. We apply a modified double-exponential method of analysis to determine τ_1, by separating the contributions of internal and external motions to the relaxation spectrum in the intermediate qR_g region. We have investigated the dynamic light scattering properties of dilute solutions of narrow distribution polystyrenes in THF and ETBZ at 25 °C in the range $1 < qR_g < 6$. The experimental quantities of interest are the infinite dilution translational diffusion coefficient, D^0_t, the relative amplitude of the pure diffusive mode, $P_0(X)/P(X)$, and the collective intramolecular relaxation time τ_c. These parameters have been used to test molecular theories on the dynamics of a single polymer chain.

Experimental Section

Narrow distribution PS samples of weight-average molecular weight, 8.42×10^6 and 20×10^6, were obtained from Pressure Chemicals (Pittsburgh) and were used without further purification. The ACS Spectrograde solvents, tetrahydrofuran and ethylbenzene, were obtained from Aldrich Chemical Co. Due to its hygroscopic nature,[40] the solvent THF was further purified by refluxing with $LiAlH_4$ for 12 h and then distilled in a dry inert N_2 atmosphere immediately before use. The solvent ETBZ was used without further purification. The refractive index of the solvents at 25 °C was determined to be $n_{25°C} = 1.407$ (THF) and $n_{25°C} = 1.495$ (ETBZ). The specific refractive index increment, dn/dc, of PS in THF and ETBZ was determined at 6328 Å and was obtained to be $dn/dc = 0.192$ and 0.111 cm³/g at 25 °C, respectively. The viscosity of the solvents was measured at 25 °C by using a Cannon Ubbelohde viscometer and was determined to be 0.465 (THF) and 0.619 cP (ETBZ). Dilute solutions of PS in THF were made by weighing individual samples in a Perkin-Elmer microbalance, Model AD-2, with an accuracy of 0.01 mg. The purified dry solvent was directly transferred into dust-free volumetric flasks containing preweighed PS samples. The solvents were equilibrated at room temperature for at least 24 h and then gently shaken for 72 h before being transferred to the light scattering cells. The method of solution preparation has been described in detail elsewhere.[39] All solutions were checked for optical clarity by monitoring the scattered intensity for 80–100 runs of 1-s duration each, and only those solutions were used where the fluctuations in the scattered intensity were less than ±2%. This ascertained the absence of dust particles or other nonhomogeneities which are sources of parasitic scattering and prevent a meaningful interpretation of the time correlation function.

Table I
Values of M_w, R_g, and R_h for Samples AD-13, AD-14, L-1, and L-2

sample	system	10^6M_w[a]	10^6M_w[b]	M_w/M_n[a]	R_g, Å	R_h, Å
AD-13	PS/THF	8.42	8.32	1.17	1356	1086
AD-14	PS/THF	20.0	22.0	1.2	2435	1946
L-1	PS/ETBZ	8.42	8.42	1.17	1608	1068
L-2	PS/ETBZ	20.0	22.0	1.2	2461	1588

[a] Suppliers specifications. [b] Measured values.

All scattering experiments were performed on a Brookhaven Instrument Corp. spectrometer comprising a BI 2000 goniometer and a BI 2030 AT correlator with a SpectraPhysics 15-mW He/Ne laser (λ = 6328 Å). Cylindrical sample cells were used and mounted at the center of a temperature-controlled, refractive index matched bath. Temperatures were controlled at 25 ± 0.1 °C for all experiments. Absolute calibration of the spectrometer was made with benzene (Spectro-grade, Aldrich Chemicals). The four systems labeled AD-13, AD-14, L-1, and L-2 were characterized by methods of static and dynamic light scattering in our laboratory. These results have been reported previously[37-39] and are summarized in Table I. For measurements of the intensity autocorrelation function, $C(\tau)$, the BI 2030 AT, 264-channel, 4-bit correlator has a multiple sampling time option enabling one to probe, simultaneously, relaxation processes occurring on widely differing time scales. This permits an accurate determination of the form of the decay rate distribution function, $G(\Gamma)$. For an optimal analysis, a large number of data points are required in the first $1/e$ part of the decay and comparatively few points which show complete decay. Correlation data are collected on several time scales simultaneously by dividing the correlator channels into four groups, each consisting of 64 equally spaced channels. Successive groups of 64 channels have sample times equal to 2^n times the sample time of the first group, where n = 0,1,2,...,8. Thus, data at four different sampling rates are collected in real time, and the data collection is 100% efficient at all sample times; i.e., no data are lost in waiting for the next group of sample times. Also, since there is great flexibility in the choice of four sample times, groups of channels can be selected such that optimal information about the fast and slow decay modes can be obtained from a give correlation function. In addition, 8 long time delay channels are available, located at 1024 times the delay increment of channel 264, and these are used in base-line determination. Typically, in our experiments 10^8 samples gave sufficiently low base-line noise. Only those intensity–intensity time correlation functions, $C(\tau)$, where the difference between the calculated and measured base lines was less than 0.1% were used for data analysis. Dynamic measurements were repeated at least twice to check for reproducibility and were found to be within 2–4% of each other. The data were further analyzed on an IBM/AT computer and a VAX 11/780.

The intensity autocorrelation function of the scattered light was measured for various combinations of concentrations and scattering angle (θ = 20–120°). At scattering wavevectors $qR_g < 1.0$, the scattered electric field autocorrelation function for monodisperse particles undergoing Brownian diffusion is

$$g^1(\tau) = \exp(-D_tq^2\tau) \quad (2)$$

where D_t is the translational diffusion coefficient and q is the magnitude of the scattering vector given by

$$q = \frac{4\pi n_0 \sin \theta/2}{\lambda} \quad (3)$$

with n_0 being the index of refraction, λ the wavelength of the incident light, and θ the scattering angle. For noninteracting spheres, the Stokes–Einstein equation gives

$$D^{\circ}_t = kT/6\pi\eta_o R_h \quad (4)$$

where k is the Boltzmann constant, T is the absolute temperature, R_h is the hydrodynamic radius of the particle, and η_o is the solvent viscosity. The concentration dependence of the translational diffusion coefficient can be obtained from

$$D_t = D^{\circ}_t(1 + k_D c) \quad (5)$$

where k_D can be evaluated by

$$k_d = 1/D^{\circ}_t(dD_t/dc)_T \quad (6)$$

By contrast, in the regime $qR_g > 1$, the correlation function becomes increasingly nonexponential due to contributions from intramolecular motions, and multimodal line-width distributions are obtained. Equation 2 can then be represented as an integral sum of exponential decays

$$|g^1(\tau)| = \int_0^\infty G(\Gamma) \exp(-\tau\Gamma)\, d\Gamma \quad (7)$$

where Γ is the decay constant corresponding to particles of a given size. The distribution $G(\Gamma)$ represents the relative intensity of light being scattered with decay constant Γ and is a function of the number and size of the scattering particles. Then, for photocounts obeying Gaussian statistics, the measured intensity–intensity correlation function $G^2(\tau)$ can be related to $g^1(\tau)$ by

$$G^2(\tau) = A(1 + b|g^1(\tau)|^2) \quad (8)$$

where A is the background (or the base line) and b is a constant that is a function of the detecting optics and accounts for the nonideal point detector. The initial decay rate is equivalent to the average value, Γ_e, of the line-width distribution function, $G(\Gamma)$

$$\Gamma_e = \int_0^\infty G(\Gamma)\Gamma\, d\Gamma \quad (9)$$

In principle, $G(\Gamma)$ can be computed by Laplace inversion of $g^1(\tau)$ in eq 7. However, in practice, the correlation function contains noise, and Laplace inversion, then, becomes a very difficult ill-conditioned problem. Hence, performing the inversion of the Laplace transform to obtain $G(\Gamma)$ was, until recently, thought to require data of unattainable accuracy. However, several approximation procedures[19-29] have been developed which can be used to obtain the form of $G(\Gamma)$. In this work, we obtained an estimate of the $G(\Gamma)$ function by using the multiexponential (MEXP) sampling technique from which values of Γ_e could be determined (within 1%). The MEXP method approximates $G(\Gamma)$ by a set of logarithmically spaced discrete single exponentials[27,28]

$$G(\Gamma) = \sum_j P_j \delta(\Gamma - \Gamma_j) \quad (10)$$

where P_j's are the weighting factors of the δ function and

$$\sum_j P_j = 1 \qquad \text{(normalization condition)}$$

$$\Gamma_j/\Gamma_{j-1} = K \qquad (K = \text{constant})$$

Substituting for $G(\Gamma)$ in eq 7 yields

$$|g^1(\tau)| = \sum_j P_j \exp(-\Gamma_j\tau) \quad (11)$$

where each of the P_j contributions are linearly independent. Following the procedure of Ostrowsky et al.,[27,28] the correlation function can be sampled at a series of linearly or exponentially spaced sample times, τ_i, and it has been shown[27] that the Nyquist sampling theorem can be applied together with an interpolation procedure[28] to fully reconstruct the correlation function at all values of τ limited only by the bandlimit ω_{max}. The experimental noise in the $G^2(\tau)$ data defines ω_{max}, which is a relative measure of the resolution of the obtained fit; i.e., $G(\Gamma)$ cannot be resolved at points closer than π/ω_{max}. Hence, the higher the value of ω_{max}, the better the resolution in $G(\Gamma)$. In this computation, the amplitude, a_i, of the highest peak corresponding to some decay constant, Γ_i, is set to 100. The rest of the amplitudes are then normalized, and any a_i's smaller than 1/200 of the highest peak are set to zero. Finally, according to the method of least squares, we minimize the fitting error of the computed function to the observed one

$$\sum_{i=1}^{M}(G^2(\tau) - \sum_{n=1}^{N} a_n \exp(-\Gamma_i\tau))^2 \quad (12)$$

and a semilog plot of the fitted values of a_n versus Γ is obtained. The initial guesses for the MEXP sampling analysis are determined first by performing a cumulant fit to obtain approximate values of Γ_e. The final estimations of the average decay rate, Γ_e, are then obtained with high precision from the MEXP analysis, and in addition, we obtain a bimodal distribution of relaxation rates, Γ_i, from which the slow relaxation mode $\bar{\Gamma}_1$ and the second mode $\bar{\Gamma}_2$ can be extracted. The accuracy of the two modes obtained from the MEXP technique was tested by using simulated biexponential data and experimental data on a mixture of monodisperse polystyrenes of weight-average molecular weights 3.84×10^6 and 5.48×10^6. We found that Γ_e was obtained within 1% and that $\bar{\Gamma}_1$ and $\bar{\Gamma}_2$ for the two modes could be accurately determined within 3–5%.

However, it has been suggested[41] before that, even for monodisperse samples, the MEXP method may show false peaks in the $G(\Gamma)$ function. This situation is made worse when the polymers have even a small degree of polydispersity.[42] We have therefore followed the suggestion of Stock and Ray[41] and have applied a double-exponential fitting (DEXP) analysis, in conjunction with the MEXP method, to resolve the $G(\Gamma)$ distribution into two modes. Here, the $G(\Gamma)$ distribution is approximated by a weighted sum of two Dirac δ functions

$$G(\Gamma) = a_1\delta(\Gamma - \Gamma_1) + a_2\delta(\Gamma - \Gamma_2) \quad (13)$$

which corresponds to

$$|g^1(\tau)| = [a_1 \exp(-\Gamma_1\tau) + a_2 \exp(-\Gamma_2\tau)] \quad (14)$$

where a_1 and a_2 are the amplitudes of the scattered intensity corresponding to the characteristic line widths Γ_1 and Γ_2. Therefore, $a_1 + a_2 = 1$ and $\Gamma_e = a_1\Gamma_1 + a_2\Gamma_2$. In the DEXP analysis we used, Γ_e was constrained to values obtained from the MEXP technique, and bimodal fits were made by using an equally weighted, nonlinear regression procedure according to Marquardt.[43] We tested this method of analysis using simulated data and found that the original bimodal distribution could be recovered by optimum fits with an accuracy of 99%.

The rationale for the DEXP analysis is that, as shown by Pecora,[10] the first-order correlation function can be written[10,15,16] as

$$g^1(\tau) = P_o(X) \exp(-Dq^2\tau) + P_2(X) \exp[-(Dq^2 + 2/\tau_1)\tau] + \ldots \quad (15)$$

where $X = q^2R_g^2$, τ_1 is the normal mode of motion of the Gaussian coil, and $P_o(X)$ and $P_2(X)$ are the dynamic form factors. Hence, the slow mode, Γ_1, can be related to the z-average translational diffusion coefficient

$$\Gamma_1 = \langle D_t\rangle_z q^2 \quad (16)$$

and τ_1 can be computed from

$$\Gamma_2 - \Gamma_1 = +2/\tau_1 \quad (17)$$

However, it is evident that the output of each computation is heavily weighted by the initial guesses supplied to the program. For example, since the values of Γ_1 and Γ_2 are highly correlated, if too large a value of Γ_1 is given as an initial guess, then an essentially meaningless distribution is obtained that contains amplitudes of negative heights. This implies that the fit of the computed values to the observed data does not converge, and hence, different initial guesses must be given to obtain a successful fit. The initial guesses for our analysis were obtained from the $\bar{\Gamma}_1$ and $\bar{\Gamma}_2$ values derived from the MEXP technique. These parameters were useful in reducing the total time taken for the curve fitting computation. The relative fitting error or the fit residuals were calculated by

$$R = \frac{G^2(\tau) - G^2(\tau)_c}{G^2(\tau)} \quad (18)$$

where $G^2(\tau)_c$ is the obtained fit. The fits were accepted if there was no systematic deviation of the residuals and the errors were less than 0.5%. In this paper, we computed several equally optimum fits for each set of experimental data, and we used the

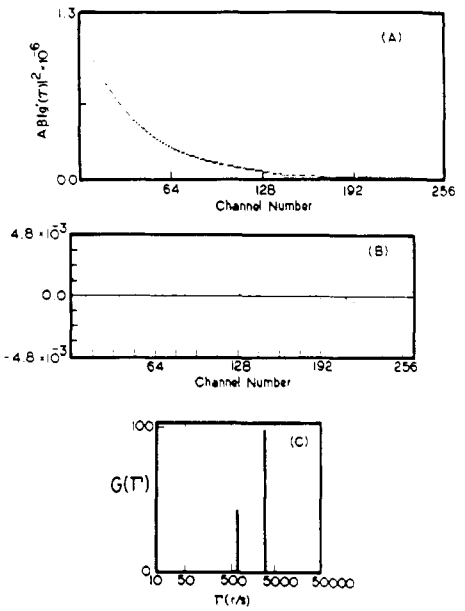

Figure 1. (A) Example of a normalized correlation function for the solution of the highest molecular weight sample (AD-14) in THF with $c = 6.09 \times 10^{-5}$ g cm^{-3} at $\theta = 50°$ and $\tau_1 = \tau_2 = 35$ μs, $\tau_3 = 70$ μs, $\tau_4 = 140$ μs. (B) Plot of the residuals versus channel number. (C) The distribution for $G(\Gamma)$ versus Γ.

results to estimate the statistical error of the computed fit. Using the above, we were able to obtain final results where the first mode, Γ_1, was consistent with $D\mathbf{q}^2$ at the different scattering angles measured. The final results for Γ_1, Γ_2, and a_1 were obtained with good precision; we estimate the errors on Γ_1 and Γ_2 to be within ±3% and for a_1 to be within ±5%.

Results

Table I summarizes results for M_w, $R_{g,z}$, and $R_h \equiv \langle R_h^{-1}\rangle_z^{-1}$ for samples AD-13, AD-14, L-1, and L-2. Figure 1A gives a typical example of a normalized autocorrelation function obtained for a solution of the highest molecular weight sample (AD-14) in THF with $c = 0.0609 \times 10^{-3}$ g/cm^3 at a scattering angle of $\theta = 50°$. Parts B and C of Figure 1 show the result of a double-exponential fit on these data together with a plot of the corresponding residuals. The excellent quality of these fits indicates that the effect of sample polydispersity is small.[42] The parameters obtained were $\Gamma_1 = 362$ rad/s, $\Gamma_2 = 1376$ rad/s, $a_1 = 0.43$, and $\Gamma_e = 940$ rad/s. A similar analysis was performed for $G^2(\tau)$ data obtained at other scattering angles and concentrations. At a given concentration, $\Gamma_1/\sin^2\theta/2$ is essentially independent of scattering angle and can be interpreted to provide an estimate of the diffusion coefficient, $\langle D_t\rangle_z$, from eq 16. This was then extrapolated to infinite dilution to obtain $\langle D^0_t\rangle_z$ and k_d from eq 5.

Similarly, the quantity $\Gamma_2 - \Gamma_1$ was obtained for each sample, at a specified scattering angle, θ, as a function of concentration, c. The values for $\Gamma_2 - \Gamma_1$ were determined within an error of 8%. We could not extract the values Γ_1 and Γ_2, with any degree of precision for $X > 10$ since the bimodal distribution obtained did not yield $\Gamma_1 = D\mathbf{q}^2$. In such cases, we did not extract Γ_1 and Γ_2 but only made an estimate of Γ_e. The values for $\Gamma_2 - \Gamma_1$ for $X < 10$ were found to be independent of concentration for all the samples, and hence the average value for all the samples was taken as $(\Gamma_2 - \Gamma_1)_{c=0}$. The latter quantity depends strongly on $\mathbf{q}$, and at higher angles this reflects contributions from higher modes of internal motions as shown in Figure 2. The limiting value of $(\Gamma_2 - \Gamma_1)_{c=0}$ was determined at $\mathbf{q}R_h = 1.0$, and this value was compared to the theoretical τ_1.

The amplitude of the translational diffusive mode relative to the total mode, P_o/P, was estimated from the

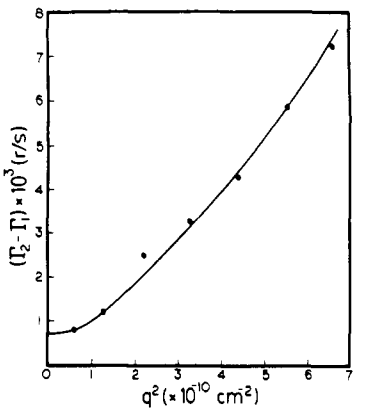

Figure 2. Angular dependence of $\Gamma_2 - \Gamma_1$ at infinite dilution for sample L-1 at 25 °C.

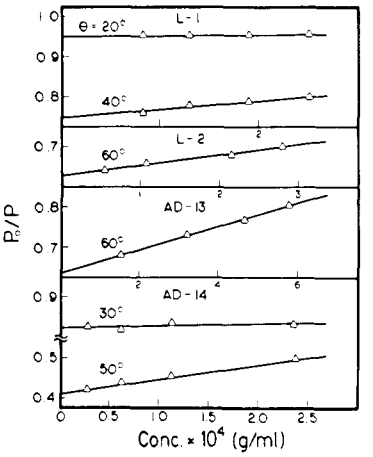

Figure 3. Concentration dependence of the dynamic form factor $P_o(X)/P(X)$ for samples AD-13, AD-14, L-1, and L-2.

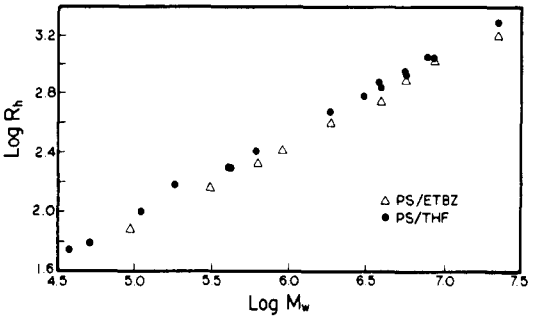

Figure 4. Logarithmic plot of the hydrodynamic radius, R_h, against the weight-average molecular weight, M_w, for PS in THF and ETBZ.

contribution of the slow component to the bimodal distribution by analyzing $G^2(\tau)$ data for a given concentration and scattering angle in the range $1 < X < 10$. Figure 3 shows some typical results for the concentration dependence of P_o/P for samples AD-13, AD-14, L-1, and L-2. As the representative samples in Figure 3 show, the P_o/P values at each angle are well represented by equations linear in c. Note that the slope of the lines in Figure 3 increases with increasing X. Extrapolation to zero concentration gives the angular dependence of the single-chain $P_o(X)/P(X)$ values for PS in THF and ETBZ which are discussed later (Figure 7).

Discussion

(a) Translational Diffusion Coefficient. In Figures 4 and 5, we compare log–log plots of R_h and R_g versus molecular weight for PS in THF and in ETBZ. All our

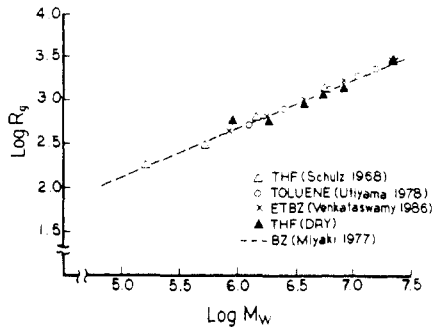

Figure 5. Logarithmic plot of the radius of gyration, R_g, versus the weight-average molecular weight, M_w, for PS/THF and PS/ETBZ.

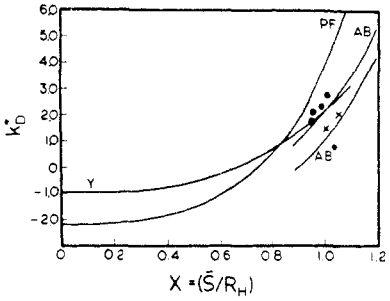

Figure 6. Diffusion virial coefficient, k_d*, plotted versus X, the ratio of the equivalent thermodynamic radius, S, to the equivalent hydrodynamic radius, R_h, in the good solvent regime: (●) PS/THF; (×) PS/ETBZ. The solid lines Y, PF, AB, and AB* are the theoretical curves in eq 21, 22, and 23.

R_h data for PS in THF fall on a line that can be best represented by the following least-squares fit:

$$R_h = (0.1569 \pm 0.01)M_w^{0.556}\ (\text{Å}) \quad (19)$$

while the data for PS in ETBZ can be represented by

$$R_h = (0.1381 \pm 0.01)M_w^{0.551}\ (\text{Å}) \quad (20)$$

On the other hand, for R_g, we find the data for PS in THF as

$$R_g = (0.161 \pm 0.01)M_w^{0.570}\ (\text{Å}) \quad (21)$$

and for PS in ETBZ as

$$R_g = (0.152 \pm 0.01)M_w^{0.579}\ (\text{Å}) \quad (22)$$

In Figure 5 we also include R_g data for PS in other good solvents. The exponents in eq 19 and 20 are slightly smaller than those determined for the R_g versus M_w relationships for the above solvent systems. Similar discrepancies have been observed in experiments on PS in benzene[2,44] and PS in toluene.[45,46] Weill and des Cloizeaux[47] have proposed that an explanation for these observations may be that the hydrodynamic radius does not reach its asymptotic molecular weight dependence nearly as fast as the radius of gyration.

We next compare experimental results for the concentration dependence of the translational diffusion coefficient, k_d, with various theoretical predictions in Figure 6. Here the data are displayed as the volume fraction coefficient k_d* ($=k_d/(N_A v_h/M)$), where $v_h = 4\pi R_h^3/3$ is the volume of the equivalent hydrodynamic sphere and N_A and M have the usual meaning. The theoretical expressions have been framed in terms of the dimensionless ratio $\tilde{X} = S/R_h$, where S is an effective hard sphere radius, calculated from the second viral coefficient $A_2 = 16\pi^2 N_A S^3/3M^2$. In Figure 6, curve Y represents the result of Yamakawa[48] using the bead-spring model:

$$k_d^* = 3.2\tilde{X}^3 - 1 \quad (23)$$

Table II
Values of $X^{1/2}$ and P_o/P at Infinite Dilution for Samples AD-13, AD-14, L-1, and L-2 at 25 °C

sample	$X^{1/2}$	$P_o(X)/P(X)$	sample	$X^{1/2}$	$P_o(X)/P(X)$
AD-13	0.9806	0.960	AD-14	1.181	0.913
	1.450	0.893		1.759	0.823
	1.894	0.733		2.326	0.606
	2.306	0.598		2.872	0.411
	2.679	0.513	L-2	1.279	0.9513
	3.104	0.436		1.905	0.833
L-1	1.235	0.957		2.517	0.745
	1.827	0.850		3.112	0.602
	2.386	0.792			
	2.906	0.625			

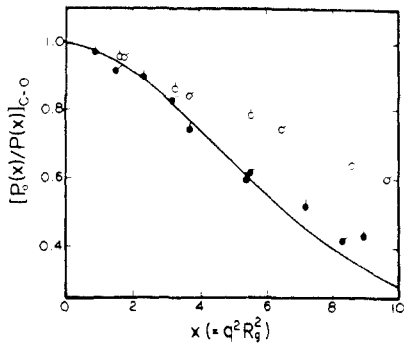

Figure 7. Plot of the reduced values $P_o(X)/P(X)$ against X ($=\mathbf{q}^2R_g^2$). Shown are the data for samples AD-13, (♦), AD-14 (●), L-1 (δ), and L-2 (σ). The solid line is the theoretical curve for nondraining Gaussian chains with preaveraged (PA) Oseen hydrodynamic interactions.

Curve PF is the equation of Pyun and Fixman[49] based on an interpenetrable porous sphere model:

$$k_d^* = 8\tilde{X}^3 - 7.16 + K \quad (24)$$

Akcasu and Benmouna[50] derived an expression for the variation of k_d* with X from the intermediate scattering function $S(\mathbf{q},t)$ and obtained curve AB:

$$k_d^* = 8\tilde{X}^3 - 6\tilde{X}^2 \quad (25)$$

Van den Berg and Jamieson[51] suggested a modification to the above by making a reference frame correction to eq 25 and obtained curve AB* where $k_d^* = 8\tilde{X}^3 - 6\tilde{X}^2 - 1$. Our experimental results indicate that the data for PS/THF are located near the curve by Yamakawa, while the PS/ETBZ results fall near curve AB*. These observations are consistent with earlier conclusions that the good solvent limit ($\tilde{X} > 0.9$) is best described by the Yamakawa and the Akcasu-Benmouna theories. We note, however, that these models do not formally incorporate such effects as variations in the strength of the excluded volume and hydrodynamic interactions.

(b) Relative Amplitude of the Translational Diffusive Mode. The variation of $[P_o(X)/P(X)]_{c=0}$, the amplitude of the translational diffusive mode with respect to the total scattered intensity, is plotted versus X ($=\mathbf{q}^2R_g^2$) in Figure 7 for both polymer solvent systems. Table II lists the $P_o(X)/P(X)$ values for samples AD-13, AD-14, L-1, and L-2. The solid line shown in Figure 7 is the theoretical[15,16] curve obtained for nearly nondraining Gaussian chains (draining parameter, $h^* = 2.67$; number of beads, $N = 100$) with preaveraged Oseen hydrodynamics. Our data for both PS in THF and ETBZ lie close to the solid line for $X < 3$. However, for $X > 3$, the P_o/P data for PS in ETBZ become systematically larger than the theoretical values. On the other hand, the data for PS in THF are always close to the solid line for all $X < 7$. Previous experimental results for the good solvent systems PS in

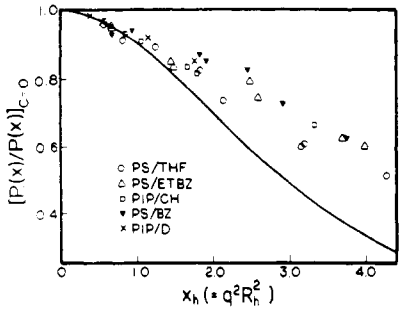

Figure 8. Reduced values $P_o(X)/P(X)$ plotted against X_h (= $q^2R_h^2$) for PS/THF and PS/ETBZ. Also included are data for PS/BZ (▼), PIP/CH (○), and PIP/1,4-dioxane (×). The solid line has the same meaning as in Figure 7.

benzene[2] and polyisoprene (PIP) in cyclohexane (CH)[3] show behavior similar to that seen for PS/ETBZ in Figure 7. On the other hand, previous results for the Θ solvent system PS in *trans*-decalin[4] are close to the theoretical curve in Figure 7 and hence are similar to our data for PS in the good solvent THF. It is pertinent to note that the differences seen in Figure 7 are qualitatively consistent with the predicted effect of variations in the strength of the hydrodynamic interaction.[15,16] Specifically, a decrease in solvent draining is predicted to lead to an enhanced contribution from internal modes. Thus, the systems PS/TD and PS/THF are nearly nondraining, while PS/PZ, PIP/CH, and PS/ETBZ exhibit a significant draining effect. It is therefore interesting that the systems PS/ETBZ, PS/BZ, and PIP/CH, which all show similar behavior of P_o/P versus X, also have comparable values of the ratio ρ ($\simeq$1.55). Likewise, the systems PS/THF and PIP/TD, whose P_o/P curves are similar, again show comparable values of ρ ($\simeq$1.3). Thus, the results of $P_o(X)/P(X)$ and ρ are consistent in suggesting that PS/ETBZ shows a larger draining effect than PS/THF.

It has been noted before[46] that selection of $\mathbf{q}R_h$ rather than $\mathbf{q}R_g$ as a scaling parameter for the angle dependence of the dynamic light scattering spectrum appears to provide a more systematic scaling parameter for the mean decay rate, Γ_e, between different polymer–solvent systems. We have therefore displayed in Figure 8 our experimental results on the quantity P_o/P as a function of $(\mathbf{q}R_h)^2$ and included, for comparison, literature data on the good solvent systems PS/benzene (ref 2) and PIP/CH (ref 3) and the Θ solvent system PS/*trans*-decalin (ref 4). The values of ρ used to convert $\mathbf{q}R_g$ values to $\mathbf{q}R_h$ were obtained from the references noted above. Figure 8 shows an approximate superposition of all these data to produce a universal master curve, which suggests that the distribution of the total scattering amplitude between internal and external relaxation modes may be determined by the product $\mathbf{q}R_h$.

(c) Longest Intramolecular Relaxation Time. We have reported for the first time information on the behavior of the quantities $(\Gamma_2 - \Gamma_1)_{c=0} = 2/\tau_c$ for PS in THF and ETBZ in the intermediate $\mathbf{q}R_g$ region. By appropriate extrapolation to the region $\mathbf{q}R_h \simeq 1.0$, we can determine the relaxation time τ_1 by using eq 17. For comparison of our results with theoretical predictions, we note first that the relaxation time of the kth normal mode is related to the eigenvalues λ_k of the Zimm diffusion equation[18]

$$\tau_k = \beta b^2/6kT\lambda_k \tag{26}$$

where β is the friction coefficient of the bead and b is the average subchain length. Since the intrinsic viscosity is given by

$$[\eta] = N_A\beta b^2\sum\lambda_k/M\eta_0 \tag{27}$$

Table III
Values of τ_1, A_1, and κ for Samples AD-13, AD-14, L-1, and L-2

10^6M_w	sample	τ_1, μs	A_1	κ^{-1}
8.42	AD-13	1364 ± 110	1.278 ± 0.102	0.011 ± 0.002
	L-1	2491 ± 200	0.844 ± 0.068	0.018 ± 0.002
20.0	AD-14	7143 ± 570	1.287 ± 0.103	0.010 ± 0.002
	L-2	12775 ± 1020	0.843 ± 0.067	0.017 ± 0.002

where M is the molecular weight, we can use eq 26 and 27 to obtain

$$\tau_1 = M\eta_0[\eta]/A_1RT \tag{28}$$

for the first normal mode where $k = 1$ and A_1 is a dimensionless coefficient. The coefficient A_1 is a function of the hydrodynamic interactions of the polymer chains. A value of $A_1 = 1.18$ was determined in the original Zimm calculation for nondraining chains using a preaveraged Oseen tensor;[18] for free-draining chains, the Rouse model[17] gives $A_1 = 0.822$. From our experimental results for τ_1, we can evaluate A_1. The results are listed in Table III. For each molecular weight, the experimental A_1 values determined for PS/THF are larger for the system PS/THF than for PS/ETBZ. This observation is again qualitatively consistent with a larger draining effect in PS/ETBZ, if we use the Rouse and Zimm preaveraged values as a yardstick. Because these theoretical analyses have not included the excluded volume effect, we cannot make a quantitative comparison with theory.

It has also been pointed out that eq 26 leads to the relation

$$D\tau_1/\langle l^2\rangle = \kappa^{-1} \tag{29}$$

where l is the end-to-end distance and κ is a number that depends on the strength of the hydrodynamic interaction and also on the excluded volume effect. Verdier and Stockmayer[52] have carried out Monte Carlo simulations to incorporate the effects of excluded volume into the analytical theories of Rouse[17] and Zimm[18] where

$$D\tau_1/\langle l^2\rangle \simeq 0.010 \tag{30}$$

for the free-draining[17] chain without excluded volume and

$$D\tau_1/\langle l^2\rangle \simeq 0.022 \tag{31}$$

for the nondraining[18] Gaussian chain. Stockmayer et al.[52] obtain

$$D\tau_1/\langle l^2\rangle \simeq 0.022 \tag{32}$$

for a free-draining chain with excluded volume. We have compared our results with the predictions of these simulations. We utilized the generalized form of the Domb–Gillis–Wilmers configurational[53] distribution function to obtain $\langle l^2\rangle$ for a self-avoiding chain:[54]

$$W(l,n) = C_n l^a \exp[-(l/\sigma_n)^b] \tag{33}$$

$$\langle l^2\rangle = R_g(n/N)^{2\nu}[2(1+\nu)(1+2\nu)] \tag{34}$$

with $t = 2.40$, $a = 2.80$, and $t = (1-\nu)^{-1}$. Here n is the length of a polymer segment, l is the end-to-end distance of the segment, C_n is the normalization constant, and σ_n is the scaling factor. We determined values of D and R_g from the scaling relationship in eq 19–22 and used eq 34 and 29 to obtain κ. These values also are listed in Table III and are numerically of the correct order of magnitude as the simulation results. It is further evident that these values show distinct differences when comparing PS/THF and PS/ETBZ, which could be interpreted as due to a

larger excluded volume and/or a smaller draining effect in THF.

In conclusion, we find that the dynamic light scattering properties of dilute PS solutions in THF and ETBZ, extending from the small to the intermediate $\mathbf{q}R_g$ region, cannot be described quantitatively by existing theory. All three pieces of experimental evidence, ρ, $P_o(X)/P(X)$, and τ_1, are qualitatively consistent in indicating a larger draining effect in PS/ETBZ versus PS/THF. Our experimental values of the longest relaxation time, τ_1, for PS in THF are similar to values predicted by a nondraining Gaussian chain model with preaveraged Oseen hydrodynamic interaction,[18] but data for the good solvent, ETBZ, are not consistent with this theory. On the other hand, our results for ρ in PS/ETBZ are consistent with predictions for nondraining self-avoiding chains,[32] but our PS/THF data are not in agreement with this calculation. The nature of the discrepancies between these two solvent systems indicates distinct differences in the details of the internal chain hydrodynamics for PS in THF versus ETBZ. It appears that PS in THF may be closer to the asymptotic good solvent nondraining limit than PS in EBTZ. It is worth noting here that dynamic light scattering data from DNA at $\mathbf{q}R_g \gg 1.6$, a wormlike coil, have been shown to be consistent with calculation from a nearly free-draining Gaussian chain.[55] Also discrepancies between experimental data on τ_1 and R_h and prediction of the Zimm theory were recently reported by Balabonov et al.[56] To obtain definitive comparison with experiment, current hydrodynamic theory for the configurational relaxation spectrum will need to be modified to include not only nonpreaveraging of the Oseen hydrodynamic interactions as well as variations in the degree of draining chain stiffness, and excluded volume, but perhaps also effects such as internal friction[57] and hydrodynamic screening.

Acknowledgment. We thank the CWRU Materials Research Laboratory for support of this work through research award NSF DMR 86-14093.

Registry No. PS, 9003-53-6.

References and Notes

(1) Berne, B.; Pecora, R. *Dynamic Light Scattering*; Wiley: New York, 1970.
(2) Nemoto, N.; Makita, Y.; Tsunashima, Y.; Kurata, M. *Macromolecules* **1984**, *17*, 425.
(3) Tsunashima, Y.; Hirata, M.; Nemoto, N.; Kurata, M. *Macromolecules* **1987**, *20*, 1992.
(4) Tsunashima, Y.; Hirata, M.; Nemoto, N.; Kurata, M. *Macromolecules* **1983**, *16*, 584.
(5) Tsunashima, Y.; Nemoto, N.; Kurata, M. *Macromolecules* ,1983, *16*, 1184. Tsunashima, Y.; Hirata, M.; Nemoto, N.; Kanjiwara, K.; Kurata, M. *Macromolecules* **1987**, *20*, 2862.
(6) Huang, W.; Frederick, J. E. *Macromolecules* **1974**, *7*, 34.
(7) (a) McAdam, J. D. G.; King, T. A. *Chem. Phys. Lett.* **1974**, *28*, 90. (b) King, T. A.; Treadway, M. F. *J. Chem. Soc., Faraday Trans. 2* **1976**, *72*, 1473.
(8) Adam, M.; Delsanti, M. *J. Phys., Lett.* **1977**, *38*, L-271.
(9) Jones, G.; Caroline, D. *Chem. Phys.* **1979**, *37*, 187.
(10) Pecora, R. *J. Chem. Phys.* **1968**, *49*, 1032.
(11) Pecora, R. *J. Chem. Phys.* **1968**, *49*, 1036.
(12) Pecora, R. *J. Chem. Phys.* **1965**, *43*, 1562.
(13) Tagami, Y.; Pecora, R. *J. Chem. Phys.* **1969**, *51*, 3293.
(14) Pecora, R.; Tagami, Y. *J. Chem. Phys.* **1969**, *51*, 3298.
(15) Perico, A.; Piaggio, P.; Cuniberti, C. *J. Chem. Phys.* **1975**, *62*(12), 4911.
(16) Perico, A.; Piaggio, P.; Cuniberti, C. *J. Chem. Phys.* **1975**, *62*(7), 2690.
(17) Rouse, P. E. *J. Chem. Phys.* **1953**, *21*, 1272.
(18) Zimm, B. H. *J. Chem. Phys.* **1956**, *24*, 269.
(19) Gulari, E.; Gulari, E.; Tsunashima, Y.; Chu, B. *J. Chem. Phys.* **1979**, *70*, 3965.
(20) Gulari, E.; Gulari, E.; Tsunashima, Y.; Chu, B. *Polymer* **1979**, *20*, 1606.
(21) Nose, T.; Chu, B. *Macromolecules* **1979**, *12*, 1122.
(22) Chu, B.; Wu, D. Q. *Macromolecules* **1987**, *20*, 1606.
(23) Provencher, S. W. *J. Chem. Phys.* **1976**, *64*, 2772.
(24) Chu, B. *Macromolecules* **1987**, *20*, 98.
(25) Chu, B. *Polymer* **1985**, *26*, 409.
(26) Pope, J. W.; Chu, B. *Macromolecules* **1984**, *17*, 2633.
(27) Ostrowsky, N.; Sornette, D.; Parker, P.; Pike, E. R. *Opt. Acta* **1981**, *28*, 1059.
(28) McWhirter, J. G.; Pike, E. R. *J. Phys. A: Math Gen.* **1978**, *11*, 1729.
(29) Dahneke, B. E. *Measurement of Suspended Particles by QELS*; Wiley: New York, 1983; pp 107–127. McWhirter, J. G. *Opt. Acta* **1980**, *27*, 83.
(30) Appelt, B.; Meyerhoff, G. *Macromolecules* **1980**, *13*, 657.
(31) Adam, M.; Delsanti, M. *Macromolecules* **1977**, *10*, 1229.
(32) Oono, Y.; Kohmoto, M. *J. Chem. Phys.* **1983**, *78*, 520.
(33) Mijnlieff, P. F.; Wiegel, F. W. *J. Polym. Sci., Polym. Phys. Ed.* **1978**, *16*, 245.
(34) McDonnell, M. E.; Jamieson, A. M. *J. Polym. Sci., Polym. Phys. Ed.* **1980**, *18*, 1781.
(35) Douglas, J. F.; Freed, K. F. *Macromolecules* **1984**, *17*, 2344.
(36) Douglas, J. F.; Freed, K. F. *Macromolecules* **1984**, *17*, 2354. Freed, K. F.; Douglas, J. F.; Wang, S. Q.; Perico, A. *Polymer-Flow Interaction*; AIP Conference Proceedings 137; American Institute of Physics: New York, 1985.
(37) Jamieson, A. M.; Venkataswamy, K. *Polym. Bull. (Berlin)* **1984**, *12*, 275.
(38) Venkataswamy, K.; Jamieson, A. M. *Macromolecules* **1986**, *19*, 124.
(39) Bhatt, M.; Jamieson, A. M. *Macromolecules* **1988**, *21*, 3015.
(40) Spychaj, T.; Lath, D.; Berek, D. *Polymer* **1979**, *20*, 437.
(41) Stock, R. S.; Ray, W. H. *J. Polym. Sci., Polym. Phys. Ed.* **1985**, *23*, 1393.
(42) Nash, P. J.; King, T. A. *Polymer* **1985**, *26*, 1003.
(43) Marquardt, D. S. *SIAM J. Appl. Math.* **1963**, *11*, 431.
(44) Miyaki, Y.; Einage, Y.; Fujita, H. *Macromolecules* **1978**, *11*, 1180.
(45) Utiyama, H.; Utsumi, H.; Tsunashima, Y.; Kurata, M. *Macromolecules* **1978**, *11*, 506.
(46) Wiltzius, P.; Cannell, D. S. *Phys. Rev. Lett.* **1986**, *56*(1), 61.
(47) Weill, G.; des Cloizeaux, J. J. *J. Phys. (Les Ulis, Fr.)* **1979**, *40*, 99.
(48) Yamakawa, H. *J. Chem. Phys.* **1962**, *36*, 2995.
(49) Pyun, C. W.; Fixman, M. *J. Chem. Phys.* **1964**, *41*, 957.
(50) Akcasu, A. Z.; Benmouna, M. *Macromolecules* **1980**, *13*, 409. Akcasu, A. Z. *Polymer* **1981**, *22*, 1169.
(51) Van den Berg, J. W. A.; Jamieson, A. M. *J. Polym. Sci., Polym. Phys. Ed.* **1983**, *21*, 2311.
(52) Verdier, P. H.; Stockmayer, W. H. *J. Chem. Phys.* **1962**, *36*, 227.
(53) Domb, C.; Gillis, J.; Wilmers, G. *Proc. Phys. Soc. (London)* **1965**, *85*, 625.
(54) Tsunashima, Y.; Kurata, M. *J. Chem. Phys.* **1986**, *84*, 6432.
(55) Sorlie, S. S.; Pecora, R. *Macromolecules* **1988**, *21*, 1437.
(56) Balabanov, S. M.; Ivanova, M. A.; Klenin, S. I.; Lomakin, A. V.; Molotkov, V. A.; Noskin, V. A. *Macromolecules* **1988**, *21*, 2528.
(57) Fixman, M. *J. Chem. Phys.* **1986**, *84*, 4085.